Check for updates

Quantitative analysis of the fluvial geomorphology and erosion on Hainan island: implications for the source-to-sink system in the NW South China Sea

Kai Qiu[1,2], Chao Lei[1,2]*, Chao Tang[1,2], Rong Yang[3], Sean Willett[4]
and Jianye Ren[1,2]

[1]Hubei Key Laboratory of Marine Geological Resources, China University of Geosciences,
Wuhan, China, [2]College of Marine Science and Technology, China University of Geosciences,
Wuhan, China, [3]School of Earth Sciences, Zhejiang University, Hangzhou, China, [4]Department of Earth
Sciences, Eidgenössische Technische Hochschule (ETH) Zürich, Zürich, Switzerland

The sediment delivery from Hainan island into the NW South China Sea during the
Quaternary is less well-defined. An investigation into the uplift, exhumation and fluvial
geomorphology of the Hainan island is crucial for improving our understanding on
the source-to-sink system in this region. In this study, we employed the digital
elevation analysis, the stream power incision model and the cosmogenic nuclide
isotope analysis to unravel how and why the Hainan island provide sediment to the
NW South China Sea. The results show that the average HI values of the main
catchments on the Hainan island are below 0.35, which indicates that the rivers on
the Hainan island tend to be stable. After mapping the channel steepness index of the
Hainan island, a high channel steepness index is constrained in the central and
western Hainan island. The χ analysis shows minor variations in χ values across the
Hainan island, except of the watershed between the Wanquanhe and Nandujiang
rivers, as well as that between the Changhuajiang and Nandujiang rivers, which
indicates the potential migration of the river watersheds here. In addition, we carried
out the cosmogenic nuclide ^{10}Be analysis on the river sand from the Hainan island.
The spatial distribution of ^{10}Be concentrations is identified to be high in the west and
low in the east. The catchment-averaged erosion rates are quantified to be 35 m/Myr,
42.5 m/Myr and 69.9 m/Myr for the Changhuajiang, Wanquanhe and Lingshuihe
catchments, respectively. We also estimated the sediment deliveries from the
Changhuajiang, Wanquanhe and Lingshuihe catchments to the Qiongdongnan and
Yinggehai Basins to be 0.46 Mt/yr, 0.45 Mt/yr and 0.21 Mt/yr, respectively. We
compared our results of the fluvial geomorphology analysis and erosion rate
estimates of the Hainan island with those of the Taiwan island. We concluded that
the difference of the erosion pattern and river evolution of the Hainan and Taiwan
islands may be associated with the variation of the tectonics. Our investigation on the
evolution of the Hainan island will improve our understanding on the source-to-sink
systems in the NW South China Sea.

1 Introduction

The source-to-sink system is a comprehensive framework used in earth science to describe the processes where sediments originated from source areas, transported along pathways, and finally deposited in sink areas (Allen, 1997; Sømme et al., 2009a, 2009b; Allen and Allen, 2013). This system is important for understanding the geological history of an area, including landscape evolution, tectonic activity and past environmental conditions. The marine basins are important sediment accumulation zones, whose source-to-sink systems have been extensively investigated to explore the links during tectonics, climate and sea-level changes (Syvitski and Milliman, 2007; Liu et al., 2016; Romans et al., 2016). The evolution of continent-scale rivers and reorganization of the plates were recorded in the continental marginal source-to-sink systems, e.g. Taiwan (Dadson et al., 2003; Chen et al., 2003; Fox et al., 2014; Derrieux et al., 2014; Chen et al., 2021) and Andes (Horton, 2018; Vergara et al., 2023). The capture between the Yangtze and Red rivers observed onshore (Clark et al., 2004) has been further studied in the marine sediments in the NW South China Sea by estimating the sedimentation rates in the offshore basins (Milliman and Farnsworth, 2011; Liu et al., 2023; Liang et al., 2023a), U-Pb dating on the zircons (Wang et al., 2014; Cao et al., 2015; Wang et al., 2016; Cheng et al., 2022) and measuring the Pb isotopes in the detrital potassium feldspar (Zhang et al., 2022a, b). However, previous studies on the source-to-sink system in the NW South China Sea did not qualify the erosion pattern of the Hainan island and reconstruct of its drainage systems, which provided sediments through rivers into the marine basins.

As a critical element of source-to-sink systems, the fluvial geomorphology serves as an essential pathway for the sediment transport (Whipple, 2004; Kirby and Whipple, 2012). With the development of the digital elevation analysis techniques, progresses have been made in the quantitative study of the fluvial geomorphology, e.g. the hypsometric curve (Strahler, 1952) and the Stream Power Incision Model (Flint, 1974).

In addition to the digital elevation analysis of the fluvial geomorphology, significant advancements have been achieved in studying their uplift and erosion processes through the isotopic geochronology (Lal, 1991; von Blanckenburg, 2005; Harel et al., 2016). Cosmogenic nuclide isotope analysis offers unique ways in estimating the erosion of the river catchments (Granger et al., 1997; Beeson et al., 2017; Bai et al., 2018; Wu et al., 2019) and assessing tectonic deformation rates (Pang et al., 2022). Specifically, the cosmogenic nuclide ^{10}Be analysis provides robust quantitative estimates of catchment-averaged erosion rates over ten-thousand-year timescales (Beeson et al., 2017; Bai et al., 2018; Wu et al., 2019).

Previous studies on the geomorphological evolution of the Hainan island primarily focuses on the river terraces (Zhang et al., 2008), the river sediment flux (Wang and Ou, 1986), the river evolution processes (Dai et al., 2016) and the coastal geomorphology (Lin, 1995; Zhou et al., 2023). The hydrological station data (Chen et al., 1991) and sediment flux in the estuarine deltas (Li et al., 2019) were utilized in estimating the erosion rate of the Hainan island, which was strongly affected by the human

activities in the recent centuries. These fails to estimate the erosion rate in ten-thousand-year intervals.

In this study, integrated with high-precision digital elevation models for fluvial geomorphological analysis, we employed cosmogenic nuclide ^{10}Be analysis to estimate the catchment-averaged erosion rates on the Hainan island. We explored the controls of tectonic activity, climate, and lithology in the fluvial geomorphology on the Hainan island. In addition, we further evaluated the sedimentary delivery of the islands in northern South China Sea to the offshore basins during Quaternary period.

2 Geographic and geological setting

The South China Sea, which is one of the largest marginal basin in the Western Pacific, formed in the context of the Mesozoic Andean-type continental margin (Zhou et al., 1995) and the Cenozoic extension and oceanization (Barckhausen et al., 2014). Several sedimentary basins have developed along its margins, such as the Qiongdongnan, Yinggehai, Beibu Gulf and Pearl River Mouth Basins (Figure 1). The Hainan and Taiwan islands are two largest islands in the northern South China Sea, which have undergone different tectonics, especially after Pliocene. Since Quaternary, the Hainan island has been primarily influenced by the volcanism, as large amount of the Quaternary volcanic rocks occurs in the northern part of the island (Lei et al., 2009). In contrast, the Taiwan island has been predominantly influenced by arc-continent collision since ~6 Ma (Lin et al., 2003). Previous studies show that the Hainan island was a significant sediment provenance in the NW South China Sea (Clift and Sun, 2006; Lei et al., 2015; Wang et al., 2021; Liang et al., 2023a; Xu et al., 2024). The Qiongdongnan, Yinggehai, Beibu Gulf and Pearl River Mouth Basins have been imaged by seismic profiles to be Cenozoic rift basins formed after Paleogene lithospheric stretching (Lei et al., 2020). The Qiongdongnan, Beibu Gulf and Pearl River Mouth Basins are formed under an NW-SE extensional stress field, while the Yinggehai Basin is a NW-trending transform-extensional basin associated with shearing (Clift et al., 2008; Shi et al., 2011; Lei et al., 2021).

The northern South China Sea is influenced by the tropical monsoon, which is characterized by frequent typhoon activities and abundant rainfall, making the islands here with substantial surface runoff. The Hainan island exhibits a topographical pattern of high elevated central regions surrounded by lower-lying areas (Figure 1). The rivers on the Hainan island present a radial drainage system, which radiate outward from the central mountainous or hilly regions, then flowing toward the periphery and ultimately discharging into the South China Sea. The main rivers on the Hainan island are the rivers of the Nandujiang, Changhuajiang, Wanquanhe, Lingshuihe, Ninyuanhe and Zhubijiang (Figure 1). The rivers of the Nandujiang, Changhuajiang and Wanquanhe are the three largest catchments on the Hainan island, covering 46.80% of the island's total area. Additionally, the Lingshuihe, Ninyuanhe and Zhubijiang rivers also have relatively large catchments, each of which covers an area of approximately 1,000 km². The Hainan island provides a substantial amount of sediment to the South China Sea, serving as a crucial
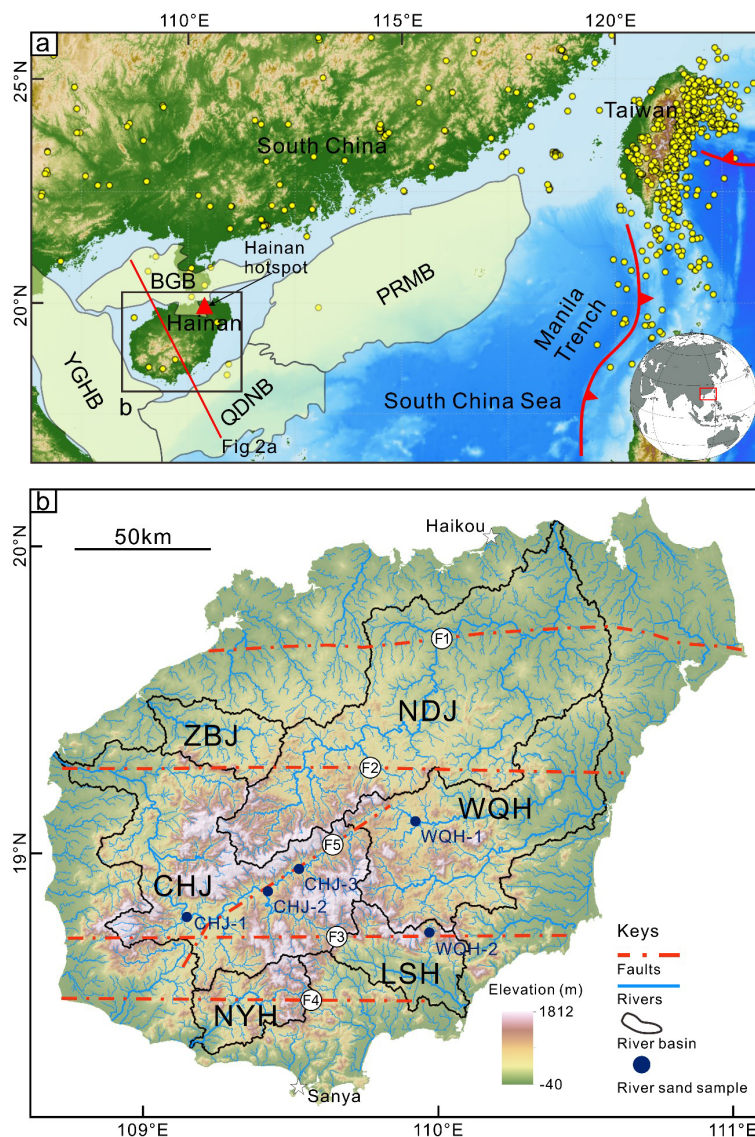
FIGURE 1
Geological background of the Hainan island and surrounding regions. **(A)** Structural Characteristics of the Hainan island and its surroundings. The solid yellow circles represent seismic activities from 2012 to 2023. The red triangle indicate the location of the volcanic vent near Haikou; **(B)** The distribution of river systems and major faults on the Hainan island. The lines shown are the faults observed in the field, i.e. Wangwu–Wenjiao Fault (F1), Changjiang–Qionghai Fault (F2), Jianfeng–Diaoluo Fault (F3), Jiusuo–Lingshui Fault (F4), Baisha Fault (F5). PRMB, Pearl River Mouth Basin; QDNB, Qiongdongnan Basin; YGHB, Yinggehai Basin; BGB, Beibu Gulf Basin; NDJ, Nandujiang river; CHJ, Changhuajiang river; WQH, Wanquanhe river; ZBJ, Zhubijiang river; LSH, Lingshuihe river; NYH, Ningyuanhe river.

source area for the Yinggehai, Qiongdongnan, Pearl River Mouth and Beibu Gulf Basins (Clift and Sun, 2006; Lei et al., 2015; Wang et al., 2021; Liang et al., 2023b; Xu et al., 2024). The erosion rate of the Nandujiang river, the largest river on the Hainan island, is estimated to be ~0.6 Mt/yr (Chen et al., 1991). The sediments transported by the Nandujiang river are carried through the Qiongzhou Strait by coastal and surface currents, and subsequently were deposited in the Beibu Gulf Basin (Liang et al., 2023b). The Changhuajiang river, the second largest river on the Hainan island, has an erosion rate of ~0.97 Mt/yr (Chen et al., 1991), serving as a significant sediment source for the Yinggehai Basin (Wang et al., 2014; Lei et al., 2015; Wang et al., 2016). The Ninyuanhe and Zhubijiang rivers offered sediments to the Yinggehai and Beibu Gulf Basins, respectively. The Wanquanhe

and Lingshuihe rivers flow towards the southeastern Hainan island, where the sediments are estimated to be transported along the continental shelf to the deep-sea plain of the Qiongdongnan Basin (Figure 2), forming submarine fan systems (Cao et al., 2015; Liu et al., 2023). Sediments from the small rivers on the NE Hainan island are transported by the offshore currents into the western Pearl River Mouth Basin (Lin, 1995; Liu et al., 2016).

The Hainan island preserves a wealth of geological records from the Indosinian tectonic movement, characterized by predominant EW and NE fault systems. The EW-striking fault system includes the Wangwu-Wenjiao Fault, Changjiang-Qionghai Fault, Jianfeng-Diaoluo Fault and Jiusuo-Lingshui Fault. The largest of the NE-NNE fault system is the Baisha Fault. Fewer seismic activity on the
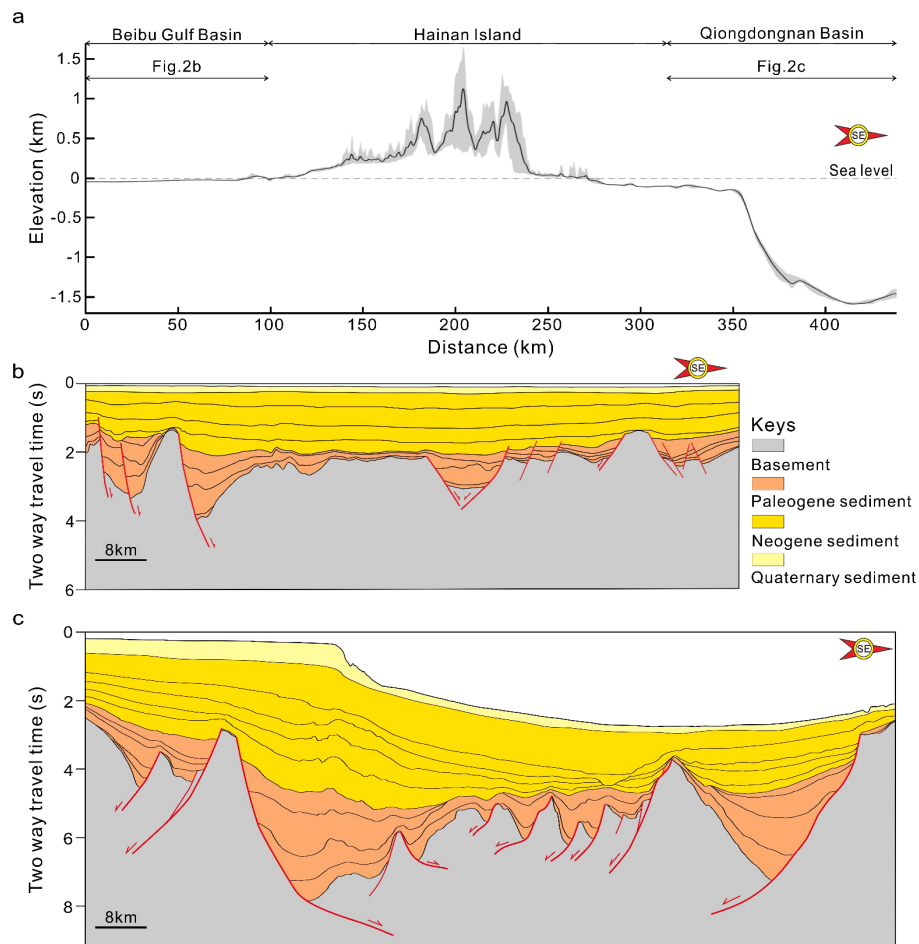
FIGURE 2
(A) Topographic profile across the Hainan island and its sedimentary basins(the profile location marked in Figure 1A); (B) The Cenozoic sediment infilling of the Cenozoic Beibu Gulf Basin [location shown in panel (A)]; (C) The Cenozoic sediment infilling of the Qiongdongnan Basin [location shown in panel (A)].

Hainan island are observed from 2012 to 2023, except of the earthquakes predominantly occurring north of the Wangwu-Wenjiao Fault and vicinity of the Jianfeng-Diaoluo Fault and Jiusuo-Lingshui Fault (Figure 1). Quaternary volcanism has been a prominent feature of the Hainan island, forming the Haikou Volcanic Group in the northern part of the island (Figure 1). In contrast to the extensive seismic activity in the Taiwan arc-continent collision zone, the earthquake on the Hainan island is relatively few to be recorded (Figure 1A).

3 Materials and methods

3.1 Fluvial geomorphology analysis

3.1.1 Hypsometric index

According to the Davis Cycle of Erosion, geomorphology is the product of the combined actions of endogenous and exogenous forces (Davis, 1899). The evolution of geomorphology can be divided into the stages of young, mature and old (Strahler, 1952; Howard, 1965; Flint, 1974). Strahler (1952) applied the hypsometric

curve to study the catchment geomorphology and defined the "Hypsometric Index" (HI) based on the shape of the curve. The HI value can be determined by several methods, e.g. the hypsometric integral curve, volume ratio or elevation-relief ratio (Strahler, 1952; Pike and Wilson, 1971). In this study, we employed elevation-relief ratio method, which approximates the hypsometric curve as the elevation-relief ratio of the terrain. The calculation formula is:

$$HI = \frac{H_{mean} - H_{min}}{H_{max} - H_{mean}} \qquad (1)$$

where H_{mean} represents the mean elevation within the catchment, while H_{max} and H_{min} denote the maximum and minimum elevations within the catchment, respectively.

According to the topography evolution and erosion of the catchment, the HI value and the hypsometric curve exhibit different characteristics at different stages of geomorphic development. During the old-age stage of geomorphic development, the HI value is relatively low (HI < 0.35), and the hypsometric curve appears concave. Conversely, during the youthful stage, the HI value is relatively high (HI > 0.6), and the hypsometric curve appears convex. The mature

stage of geomorphic development is characterized by an S-shaped hypsometric curve and an HI value that falls within the intermediate range (0.35 < HI < 0.6) (Strahler, 1952).

3.1.2 Channel steepness index

Mathematical models of fluvial erosion are useful to predicate the quantitative links between tectonic-climatic perturbations and the temporal evolution of channel geometry and drainage networks. The process of fluvial surface changing can be expressed as:

$$\frac{dz}{dt} = U - E \tag{2}$$

where z is surface elevation, t is time, U represents bedrock uplift rate and E represents erosion rate.

Among the proposed fluvial incision models, the most commonly used approach is the Stream Power Incision Model (SPIM) (Hack, 1957; Whipple and Tucker, 1999; Lague, 2014). The long-term erosion rate (E) is expressed as:

$$E = KA^m S^n \tag{3}$$

where K represents erodibility coefficient influenced by lithology and climate, S denotes the river channel slope, and A is the upstream drainage area. The parameters m and n are the drainage area and slope exponents, respectively.

In steady-state, i.e., when $\frac{dz}{dt} = 0$, river longitudinal profile can be represented as (Flint, 1974):

$$S = K_{sn}A^{-\theta} \tag{4}$$

where K_{sn} is channel steepness index, θ represents concavity index. The formula for calculating K_{sn} is expressed as:

$$K_{sn} = \left(\frac{U}{K}\right)^{\frac{1}{n}} = \left(\frac{E}{K}\right)^{\frac{1}{n}} \tag{5}$$

When n=1, channel steepness index is directly proportional to the bedrock uplift rate. Therefore, this index is often utilized to reflect the regional uplift rate (Kirby et al., 2003; Wobus et al., 2006).

3.1.3 χ value

The migration of watershed divides can be influenced by various factors, such as tectonic uplift, precipitation, rock strength and changes in the base level fall (Goren et al., 2014; Whipple et al., 2017). Perron and Royden (2013) proposed an integral method χ-plot, which is to calculate channel steepness index and display transient information on river evolution. This method provides insights into watershed migration trends, e.g. drainage reorganization and river capture (Willett et al., 2014; Yang and Goren, 2015). The calculation formula can be expressed as:

$$\chi = \int_0^x \left(\frac{A_0}{A}\right)^{\frac{m}{n}} dx \tag{6}$$

where A_0 is an area-scale factor, and in this study, $A_0 = 1$. During the migration of drainage divides, the catchment area of the capturing river increases and the χ values increase, while the drainage area of the captured river decreases, resulting in reduced χ values. The χ values on both sides of the drainage divide gradually equalize, indicating an equilibrium state of the drainage system.

Therefore, the magnitude of χ values not only indicates the migration direction of watershed, but also it signifies whether rivers are gaining or losing drainage area. This study assumes a uniform concavity index θ = 0.45 (m = 0.45, n = 1) to calculate channel steepness index and χ values (Kirby and Whipple, 2012).

3.1.4 Knickpoint

River knickpoint refers to a discontinuity in channel gradient that forms in areas with variations in lithology, faults and differential tectonic uplift (Whipple, 2001, 2004; Boulton and Whittaker, 2009; Li et al., 2021). On river profiles, it appears as a convex line with a marked increase in channel gradient downstream of the knickpoint. Consequently, the upstream and downstream river segments around knickpoints often exhibit different values of channel steepness index.

In this study, knickpoints were identified using the 'Knickpointfinder' tool from TopoToolbox (Schwanghart and Scherler, 2014). This tool analyzes river long profiles to extract knickpoints. Firstly, it extracts the entire river long profile and fits a smooth concave profile to it. Nodes on the river long profile with a Maximum Vertical Offset (Δz) exceeding the tolerance threshold (tol) are marked as knickpoints. The river segments are then divided at these knickpoints, and this process is iterated until the maximum vertical offset is less than the tolerance threshold (Schwanghart and Scherler, 2017; Sonam et al., 2021; Penserini et al., 2024). In this study, a tolerance threshold of tol = 90 was chosen to enable the planar distribution of river knickpoints on the Hainan island.

3.2 Estimating catchment-averaged erosion rates using cosmogenic nuclide ^{10}Be

The cosmogenic nuclide ^{10}Be analysis for estimating catchment-averaged erosion rates was proposed by Lal (1991). In this study, five sand samples were collected from the Changhuajiang, Wanquanhe, and Lingshuihe rivers on the Hainan island for cosmogenic nuclide ^{10}Be analysis. The sand samples, each weighed approximately 1 kg, were collected from river banks or river beds. Specifically, river samples CHJ-1, CHJ-2, and CHJ-3 were collected from the Changhuajiang river, sample WHQ-1 from the Wanquanhe river, and sample WHQ-2 from the Lingshuihe river (Figure 1B; Supplementary Figure S1). The preprocessing and testing of these sand samples were conducted at the Accelerator Mass Spectrometry (AMS) Laboratory of the Department of Earth Sciences, ETH Zürich, Switzerland.

In this study, stable isotope ^{9}Be was used to correct for the loss of ^{10}Be. First, the samples were processed to get approximately 50 grams of pure quartz and then dried, followed by dissolving and cleaning the quartz using the mixture of hydrochloric acid (HCl) and hydrofluoric acid (HF). ^{9}Be was separated from the samples using ion chromatography and chemical separation methods. The isolated ^{9}Be was converted into a positively charged ion beam, and the number of ^{9}Be ions was determined by collection and counting. The ^{10}Be/^{9}Be ratio was measured at the Accelerator Mass

Spectrometry (AMS) Laboratory (Christl et al., 2013) and normalized using the ETH standards (Nominal $^{10}Be/^9Be = 1.86 \times 10^{-14}$, Blank-ratio $^{10}Be/^9Be = 2.60 \times 10^{-15}$). The errors in this process arose from the inherent analytical errors in AMS measurements and blank error propagation (Kubik and Christl, 2010). The ^{10}Be concentrations were calculated based on the $^{10}Be/^9Be$ ratio and the previous measured ^9Be. The results through precision verification and error correction yield an average sample error of 6.72%.

4 Results

4.1 Fluvial geomorphology on Hainan island

4.1.1 Hypsometric index

The HI values of the main catchments on the Hainan island were calculated after the method shown in section 3.1.1. The averaged HI values for the Nandujiang, Changhuajiang, Wanquanhe, Zhubijiang, Lingshuihe and Ningyuanhe catchments are 0.294, 0.345, 0.288, 0.261, 0.305, and 0.327, respectively. Spatially, the HI values of the western and southern catchments (the Changhuajiang, Lingshuihe and Ningyuanhe rivers) are higher than those in the eastern and northern catchments (the Nandujiang, Wanquanhe and Zhubijiang rivers). The average HI values of all the catchments of the Hainan island are less than 0.35.

It is noteworthy that some tributaries of the Hainan island exhibit higher HI values, while most rivers have relatively lower values (Figure 3). The higher HI values are predominantly concentrated in the central hilly regions, possibly due to ongoing slow uplift. In the middle and lower reaches of the Nandujiang river,

there are high-value areas, which can be related to the presence of the Wangwu-Wenjiao Fault and the Qiongbei volcanic group (Figures 1B, 3).

The hypsometric curves of the main catchments on the Hainan island present concave shapes (Figure 4), while the HI values are primarily concentrated between 0 and 0.35 (Figure 3). According to the Davis Cycle of Erosion (Davis, 1899; Strahler, 1952), the average HI values of the catchments on the Hainan island (<0.35) indicate that these catchments are in the old-age stage of geomorphic development. This stage is characterized by small hydraulic gradients, slower river flow rates and lower erosion rates. Therefore, the riverbeds are stable, with larger downstream drainage areas and smaller upstream drainage areas.

4.1.2 Channel steepness index

The Nandujiang, Changhuajiang and Wanquanhe rivers exhibit high K_{sn} values ($K_{sn} > 80$) near their headwaters (Figure 5A), indicating relatively strong uplift associated with tectonic activity in these regions. The Changhuajiang catchment, located on south side of the Limuling Mountain, shows considerable differences in K_{sn} values with the Nandujiang catchment, located on the north side of the Limuling Mountain. This indicates that different uplift occurred across the Limuling Mountain. The downstream of the Nandujiang and Wanquanhe rivers show a noticeable decreasing trend in K_{sn} values for their tributaries, eventually stabilizing at lower values (Figure 5A).

The kernel density estimation of the K_{sn} of the main catchments on the Hainan island shows a distribution primarily between 0 and 50, with a concentration between 0 and 20 for the Nandujiang, Wanquanhe, and Zhubijiang rivers (Figure 5B). This spatial pattern of the K_{sn} indicates that the central and western regions of the
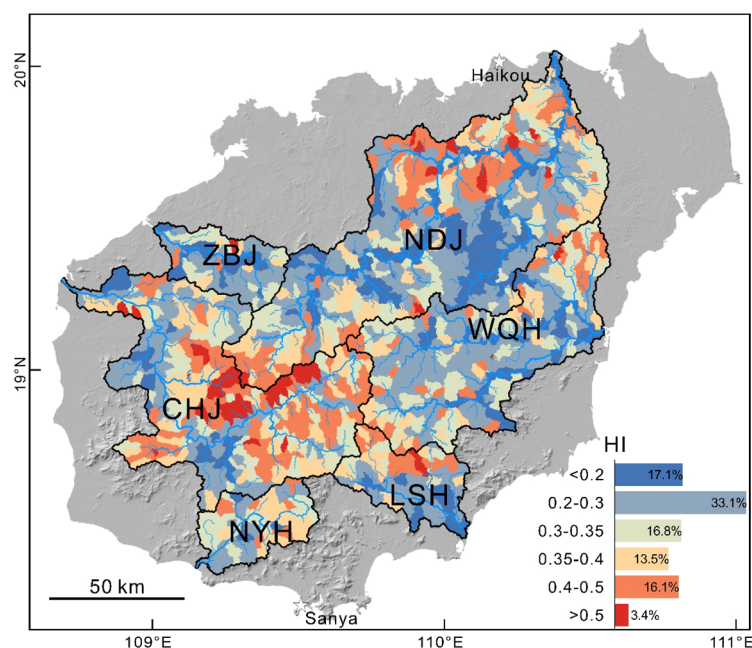
FIGURE 3
The map showing the spatial distribution of the hypsometric index for the main catchments on the Hainan island.
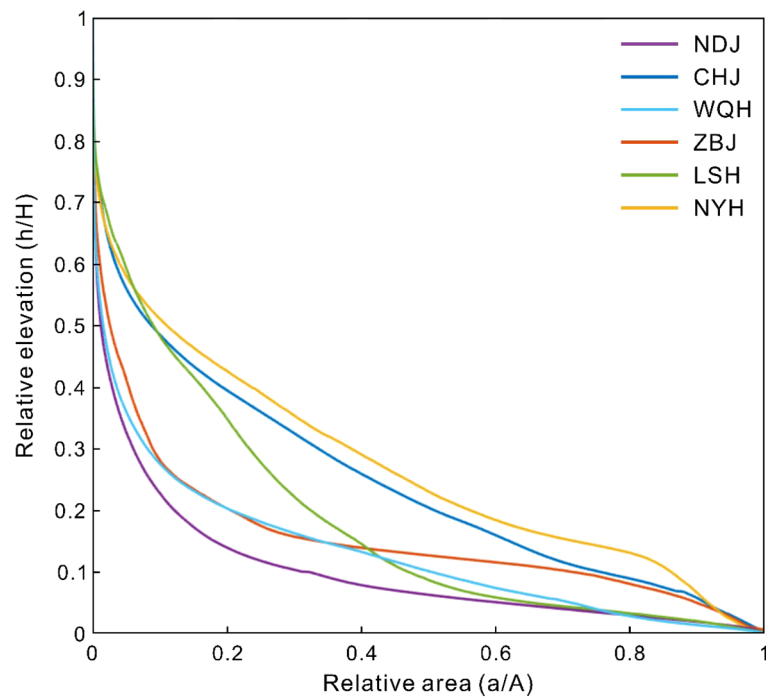
FIGURE 4
Hypsometric curve of the main catchments on the Hainan island. H is total relief within the basin (maximum elevation minus the minimum elevation), A is total catchment area, a is surface area within catchment above a given altitude(h).

Hainan island experience relatively strong tectonic uplift, while coastal areas exhibit much weaker tectonic activities. This geological configuration results in a terrain characterized by higher elevations in the central region surrounded by lower elevations, contributing to a radial drainage system where some major rivers radiate outward from the central area (Figures 1, 5).

4.1.3 χ analysis

The spatial distribution of χ values in the main catchments of the Hainan island presents differences along the watershed boundaries (Figure 6). At the divides between the Nandujiang-Changhuajiang, Wanquanhe-Lingshuihe and Changhuajiang-Lingshuihe catchments, the χ values exhibit a pattern of lower values to the south and higher values to the north (Figures 6, 7A, C, D), indicating stronger erosion capabilities on the southern side of the divides and suggesting a northward migration of the divides. This result shows higher erosion rates in watersheds to the south compared to those in the north and aligns with that observed from hydrological data (Chen et al., 1991). The divide between the Wanquanhe and Changhuajiang catchments shows a pattern of the χ values with high in the west and low in the east, but the differences are small, indicating that the migration of the catchment divide appears to be impossible (Figures 6, 7B). Overall, the χ values in the larger catchments such as the Nandujiang, Changhuajiang and Wanquanhe rivers are slightly higher than that of the Zhubijiang, Lingshuihe and Ningyuanhe rivers. However, the differences in the χ values among the main catchments are small

and primarily range between 2 and 15. Therefore, the possible divide migration on the Hainan island is not prominent.

4.1.4 Knickpoint analysis

In this study, thirty river knickpoints were identified on the Hainan island (Figure 8). They are predominantly situated at an elevation of 593 ± 191 (1σ) meters with a distance of 127.9 ± 69.4 (1σ) kilometers from the river mouth. The variations of knickpoints in elevation and migration distances suggest the presence of multiple tectonic or climatic events on the Hainan island (Goren et al., 2014; Zhang et al., 2023). The knickpoints are observed in the hilly region to the south of the Changjiang-Qionghai Fault, where the significant topographic relief and high K_{sn} values occurred (Figure 5). This observation is consistent with previous results across the world (Kirby and Whipple, 2012; Sonam et al., 2021; Li et al., 2021). Most knickpoints are located within 6 km away from the watershed divide (n=22), which shows the knickpoints migrated a long distance with small upstream drainage areas and indicates slow migration rates of the knickpoints (Loget and Van Den Driessche, 2009; Gallen and Wegmann, 2017). To the northwest of the Baisha Fault, the knickpoints are more concentrated, forming a NE-trending knickpoint zone (Figure 8). Lithological knickpoints are developed in the upper reaches of the Nandujiang river and the middle and upper reaches of the Changhuajiang river. These knickpoints are primarily located along the boundaries between Mesozoic sedimentary rocks, Paleozoic sedimentary rocks and granite, with a pronounced presence at the Mesozoic sedimentary rock-granite interface (Figure 8).
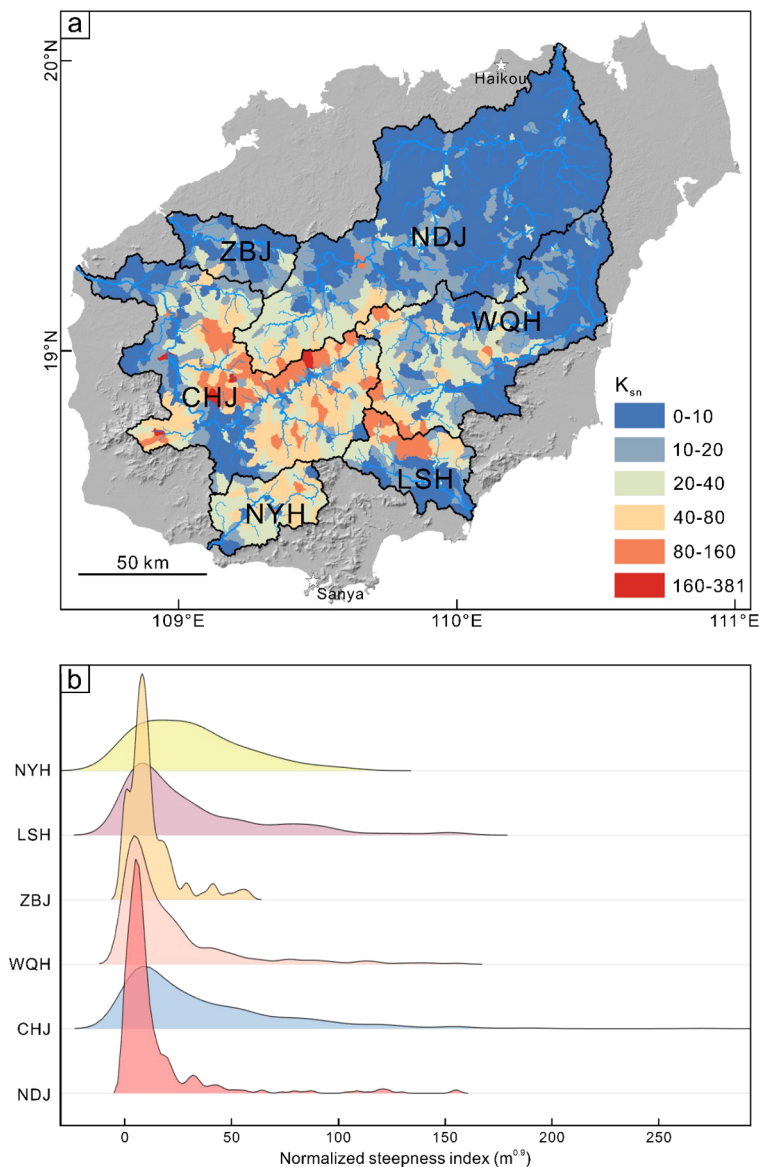
FIGURE 5
(A) Spatial distribution map of channel steepness index for the main catchments on the Hainan island; **(B)** Kernel density estimation of channel steepness index for different river catchments.

4.2 Erosion rates of the catchments on the Hainan island

In this study, we collected sand samples from the main catchments on the Hainan island and estimated the catchment-averaged erosion rates using cosmogenic nuclide [10]Be analysis. Our result indicates that the average [10]Be concentrations in the Changhuajiang, Wanquanhe and Lingshuihe catchments are 8.26×10^4 at/g, 6.61×10^4 at/g and 4.26×10^4 at/g, respectively (Table 1). The spatial distribution of [10]Be concentrations is influenced by both erosion rates and elevation. Generally, the [10]Be concentrations on the eastern Hainan island are lower than that of the western regions.

The catchment-averaged erosion rates in the Changhuajiang, Wanquanhe and Lingshuihe catchments are 35 m/Myr (9.3 mg/cm²•yr), 42.5 m/Myr (11.3 mg/cm²•yr) and 69.9 mg/

cm²•yr), respectively (Table 1). The catchment-averaged erosion rates here closely approximate the data estimated from the hydrological stations (Chen et al., 1991). The spatial distribution of the erosion rates across the Hainan island indicates an overall trend of higher rates in the east and lower rates in the west. The erosion rates in the Wanquanhe and Lingshuihe catchments are higher than those in the central hilly regions, with the highest recorded erosion rate of 69.9 m/Myr (18.5 mg/cm²•yr) in the Lingshuihe catchment (Figure 9A).

This study uses the erodibility coefficient K to quantify the relationship between topography and the catchment-averaged erosion rate over ten-thousand-year intervals (Whipple and Tucker, 1999; Kirby and Whipple, 2012), to some extent reflecting the rock's resistance to erosion. When n = 1, the result based on Equation 5 show that the Lingshuihe catchment exhibits
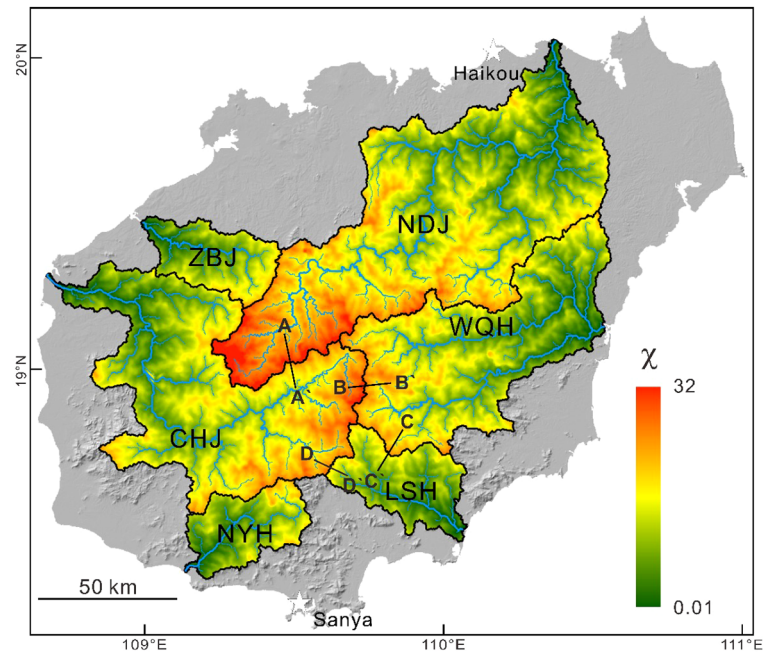
FIGURE 6
Spatial distribution map of χ value for the main catchments on the Hainan island.
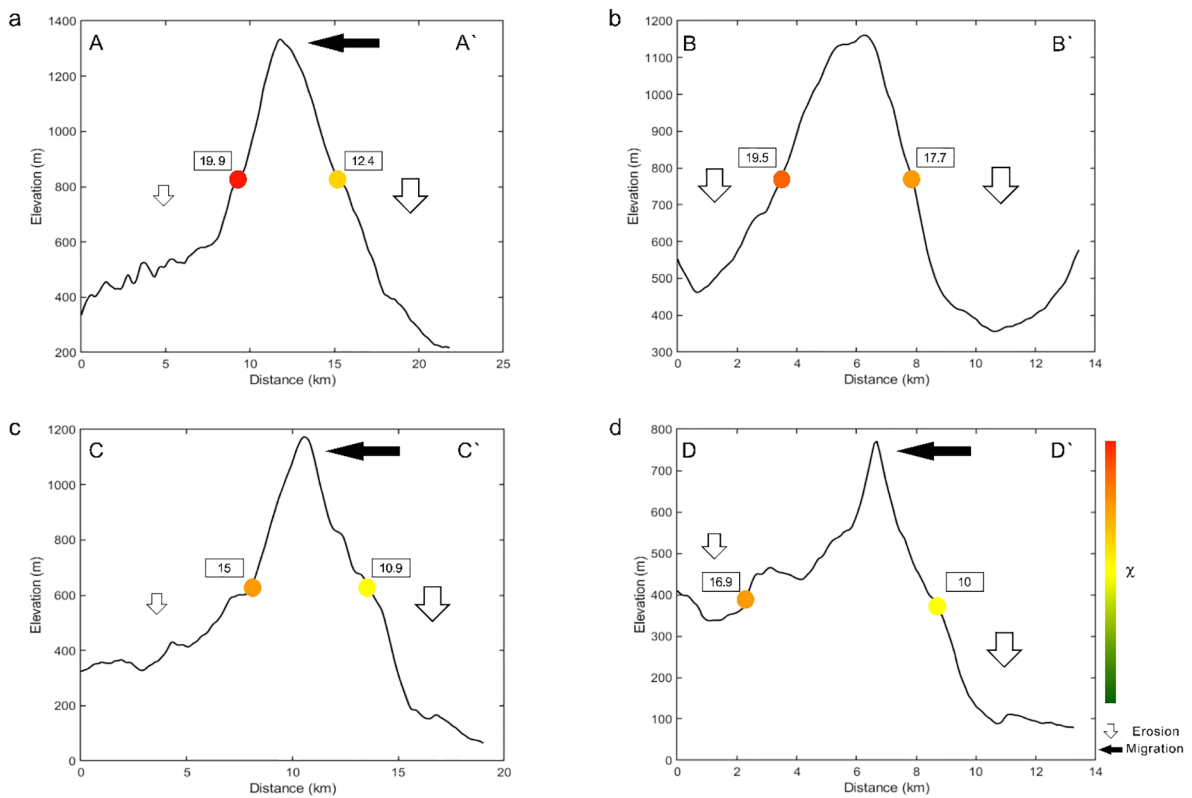
FIGURE 7
The χ values and topographic differences on both sides of the main catchment divides on the Hainan island. **(A)** Nandujiang (A) and Changhuajiang (A`); **(B)** Changhuajiang (B) and Wanquanhe (B`); **(C)** Wanquanhe (C) and Lingshuihe (C`); **(D)** Changhuajiang (D) and Lingshuihe (D`). Location of the topographic profiles are shown in Figure 6.
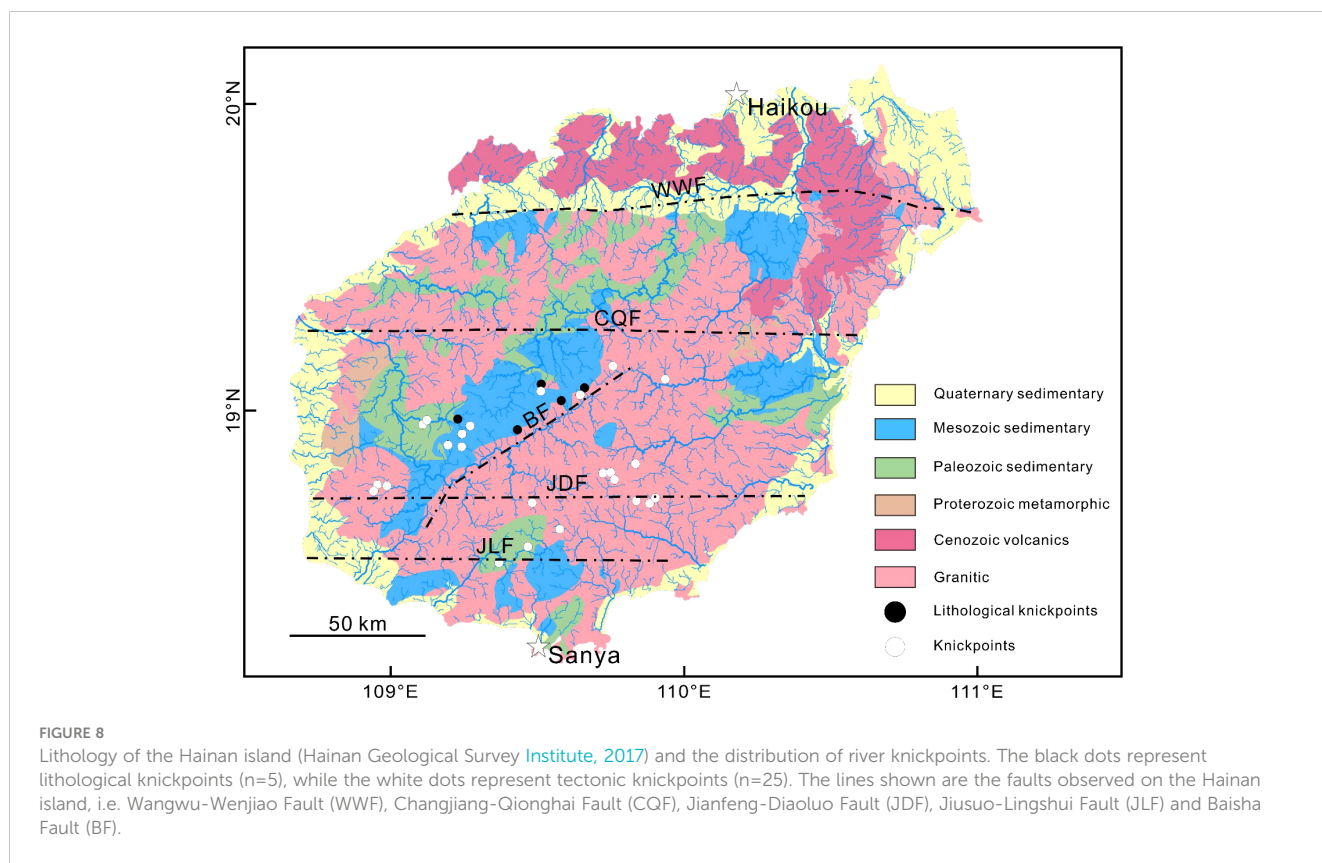
FIGURE 8
Lithology of the Hainan island (Hainan Geological Survey Institute, 2017) and the distribution of river knickpoints. The black dots represent lithological knickpoints (n=5), while the white dots represent tectonic knickpoints (n=25). The lines shown are the faults observed on the Hainan island, i.e. Wangwu-Wenjiao Fault (WWF), Changjiang-Qionghai Fault (CQF), Jianfeng-Diaoluo Fault (JDF), Jiusuo-Lingshui Fault (JLF) and Baisha Fault (BF).

the highest erodibility coefficient K, at 1.69×10^{-6} m$^{0.1}$/yr, while the Changhuajiang catchment has a lower erodibility coefficient K, at 0.88×10^{-6} m$^{0.1}$/yr. The overall distribution of erodibility K on the Hainan island resembles that of erosion rates, with higher erodibility coefficient corresponding to regions of higher erosion rates (Figure 9B).

5 Discussion

5.1 Controls of the fluvial geomorphology on the Hainan island

5.1.1 Faults and tectonic uplift

On the central Hainan island, the morphology in the upper reaches of the Changhuajiang river aligns with the orientation of the

Baisha Fault. While, the EW-trending Wangwu-Wenjiao Fault to the northern Hainan island and Jiushuo-Lingshui Fault to the southern Hainan island were active during Early to Middle Pleistocene. The morphologies in the lower reaches of the Changhuajiang river and the upper reaches of the Ningyuanhe river exhibit an EW orientation influenced by these faults (Figure 1B). The Wangwu-Wenjiao Fault was imaged seismically to cut the deep crust and remains active today (Hu et al., 2016). However, compared to the active Quaternary faulting in the Taiwan island, the magnitude and frequencies of the fault activities on the Hainan island are weaker and fewer, respectively (Hu et al., 2018). The river longitudinal profiles show that there are several sharp changes on the channel gradients, where the high-angle faults and associated waterfalls occurred (Figures 10A, B).

Differential tectonic uplift is a significant manifestation of the neotectonic activity on the Hainan island. On either side of tectonic

TABLE 1 Erosion rates from the ^{10}Be cosmogenic nuclide analysis on the river sand samples from the Hainan island.

Sample ID	Longitude	Latitude	^{10}Be concentration (10^4atoms/g)	^{10}Be/^{9}Be Ratio (10^{-12})	Error (%)	Erosion rate		Error (m/Myr)
						(mg/cm^2•yr)	(m/Myr)	
CHJ-1	109.12	18.78	10	0.204	6.24	7.08	26.7	1.74
CHJ-2	109.39	18.86	6.97	0.154	5.27	10.8	40.6	2.27
CHJ-3	109.50	18.94	7.81	0.08	7.8	10	37.8	3.26
WQH-1	109.90	19.10	6.61	0.179	4.75	11.3	42.5	2.13
WQH-2	109.95	18.73	4.26	0.076	7.28	18.5	69.9	5.68

FIGURE 9
Erosion rates Figure **(A)** and erodibility coefficient K Figure **(B)** on the Hainan island.
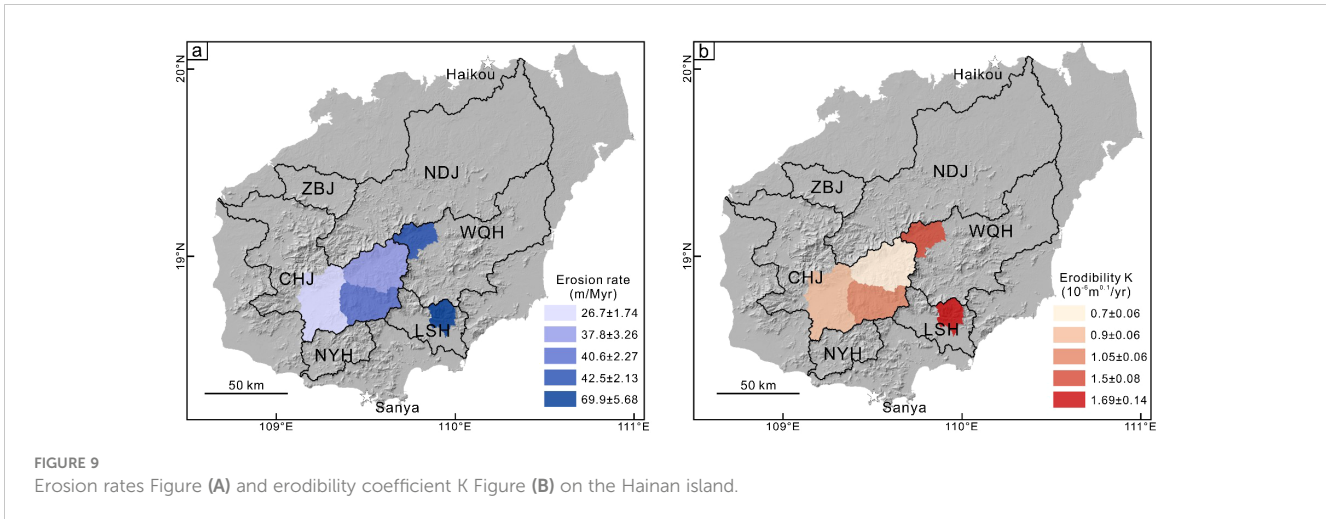
belts, the contrasting geomorphic landscapes have formed due to differential uplift and subsidence associated with neotectonic movements (Whittaker, 2012). River knickpoints have developed in the main catchments of the Hainan island (Figures 8, 10). Most of the river knickpoints are associated with differential tectonic uplift, which causes river channels steepening and incision as shown across the world (Kirby and Whipple, 2012; Li et al., 2021; Sonam et al., 2021). This highlights the intermittent slow uplift associated with neotectonic activity on the Hainan island and its impact on the river knickpoints.

5.1.2 Magmatism

Geological surveys have indicated that active Cenozoic magmatic activities occurred on the Hainan island, with extensive distribution of the alkaline basalts in the northern island (Figures 1, 8). These basalts are similar to those observed in the Leizhou peninsula, Weizhou island, Xisha islands and Indochina peninsula (Yan et al., 2008; Wang et al., 2013; An et al., 2017; Zhang et al., 2020). Geochemical analysis of these rocks exhibits typical OIB-type characteristics along with DUPAL anomalies and attributes of high mantle temperatures (Yan and Shi, 2007). Given the presence of low-velocity anomalies originating from the lower mantle beneath the Hainan island and its adjacent regions (Montelli et al., 2006; Zhao, 2007; Xia et al., 2017; Zhao et al., 2021), it can be indicated that this area is influenced by a mantle plume.

The magmatic activity induced by mantle plume has a crucial impact on the fluvial geomorphology of the Hainan island. It is noteworthy that the increased HI values of rivers occurred near the Qiongbei volcanic group (Figure 3), with some values exceeding 0.5. These elevated HI values indicate active tectonic processes in this region (Lifton and Chase, 1992; Chen et al., 2003). The magmatic activities have resulted in pronounced river incision and related geomorphic processes in this area.

5.1.3 Lithology

Different rock types exhibit varying erosion resistance and strength, which alter the fluvial erosion processes that control catchment morphology (Whipple et al., 2000; Sklar and Dietrich, 2001; Duvall et al., 2004), e.g. hillslope geometries, peak elevations, catchment and channel geometries (Baumann et al., 2018). As shown in Figure 8, the northwestern region of the Baisha Fault exhibits five lithological knickpoints, predominantly occurring at the contacts between granite and sedimentary rock. This observation aligns with the observation that the boundary between more and less resistant lithologies often form river knickpoints along the river profiles (Walsh et al., 2012). The lithological knickpoints primarily result from the erosion resistance difference between granite and sedimentary rock, which records the variations in regional tectonic activity and uplift.

5.1.4 Climate

The climate change plays an important role in modulating the river incision, thereby influencing the transient processes of fluvial geomorphology (Whittaker, 2012; Zhang et al., 2023). Previous study has shown that the knickpoints are formed by base-level fall induced by tectonic activity and/or climate change (Kirby and Whipple, 2012). Consequently, the river knickpoints on the Hainan island not only record the regional tectonics but also reflect the multiple climate change events (Goren et al., 2014; Zhang et al., 2023). The distribution of precipitation influences river morphology and erosion patterns by modulating river discharge (Kirby et al., 2003; Wobus et al., 2006). The Hainan island is situated in a region with abundant precipitation and typhoon activities (Cao et al., 2015). The distribution of erosion rates on the Hainan island resembles that of spatial pattern of the precipitation with higher rates in the east and lower in the west (Figure 9A; Supplementary Figure S2). The monsoonal climate further contributes to the disparity in erosional patterns between the windward and leeward slopes (Jiang et al., 2018) (Figures 1B, 9A; Supplementary Figure S2).

FIGURE 10
Long profiles of the main streams on the Hainan island, which highlights lithological variations with different colors. **(A)** Nandujiang;
(B) Changhuajiang; **(C)** Wanquanhe; **(D)** Zhubijiang; **(E)** Lingshuihe; **(F)** Ningyuanhe. The black solid lines represent the river longitudinal profiles,
while the blue solid lines show the distribution of channel steepness index along the rivers. River knickpoints are marked with red triangles.

5.2 Sediment delivery from the Hainan island to the surrounding basins

According to the erosion rates for the main catchments on the Hainan island (Table 1), the sediment loads to the adjacent basins from the Changhuajiang, Wanquanhe and Lingshuihe catchments are 0.46 Mt/yr, 0.45 Mt/yr and 0.21 Mt/yr, respectively. In comparison, the main catchments in the Taiwan island, such as the Cho-Shui River, Tseng-Wen River and Kao-Ping River, have significantly higher sediment loads of 54.1 Mt/yr, 25.1 Mt/yr, and 49 Mt/yr, respectively (Dadson et al.,

2003). The sediment load capacity of the Taiwan island far exceeds that of the Hainan island (Dadson et al., 2003; Milliman and Farnsworth, 2011). The substantial difference in sediment load capacity between the Hainan and Taiwan islands is likely attributed to the variations in erosion rates. The Taiwan island contributes substantially more sediments to the South China Sea compared to the Hainan island (Liu et al., 2016).

Cosmogenic nuclides in modern river sediments provide average erosion rates for catchments over time scales of 10^5 to 10^7 years (Derrieux et al., 2014; Fellin et al., 2017), offering insights into erosion processes since the Quaternary. Previous studies

estimated the Quaternary deposition rates for the Qiongdongnan and Yinggehai Basins to be ~20750 km^3/Myr (Clift and Sun, 2006) and ~25926 km^3/Myr (Lei, 2012), respectively. The densities of wet mud and wet sand are ~1.7 t/m^3 and ~1.8 t/m^3, respectively (Bai et al., 2009). The Quaternary deposition rates of the Qiongdongnan and Yinggehai Basins are estimated to be 3.5×10^{13} t/Myr and 4.5×10^{13} t/Myr, respectively.

The calculated erosion rates in the main catchments of the Hainan island indicate the sediment loads from the Changhuajiang, Wanquanhe, and Lingshuihe catchments are approximately 4.6×10^{11} t/Myr, 4.5×10^{11} t/Myr and 2.1×10^{11} t/Myr, respectively. The Changhuajiang and Ningyuanhe catchments, located in the western Hainan island, have almost similar lithological distributions (Figure 8). The erosion rates of the Ningyuanhe catchment is as same as the Changhuajiang catchment. The Quaternary sediment delivery from the Ningyuanhe catchment is estimated to be ~0.9×10^{11} t/Myr. Therefore, the sediment loads from the Changhuajiang and Ningyuanhe catchments accounts for ~1.2% of the total Quaternary deposition in Yinggehai Basin, while the Wanquanhe and Lingshuihe catchments contribute ~1.9% to the total Quaternary deposition in Qiongdongnan Basin. This study indicates that the sediment contributions of the Hainan island to the Qiongdongnan Basin is much smaller than previous study (Cheng et al., 2022). The sediment delivery from the Hainan island during Quaternary is much smaller compared to that during Miocene (Cao et al., 2015).

5.3 Uplift and erosion processes on the Hainan island

Surface processes are influenced by several factors, e.g. channel gradient, regional climate, river channel geometry and rock erodibility (Whipple, 2001; Sklar and Dietrich, 2001; Wobus et al., 2006; Jepson et al., 2021). In this study, we have shown that the river evolution and surface erosion are affected from interactions between tectonic movements and climatic changes. The Taiwan island, another island in the northern South China Sea (Figure 1A), exhibits an average erosion rate of 2361.8 m/Myr (Derrieux et al., 2014; Fellin et al., 2017; Chen et al., 2021), much larger than that of the Hainan island with an average erosion rate of 43.5 m/Myr. Compared with the global cases (Figure 11), the Hainan island shows low erosion rates and K_{sn} values. However, the erosion rates of the Taiwan island are much larger than those of other catchments worldwide, accompanied by substantial variations in its K_{sn} values (Figure 11). This stark disparity in erosion rates may be attributed to the difference of tectonic activities between the two islands.

Geological evidence shows that since Mesozoic the Hainan island experienced intense tectonic and magmatic activities (Jiang et al., 2024). The K_{sn} and HI values of the Hainan island indicates that the tectonic activities on the Hainan island is weak at present, accompanied by low uplift rates. In contrast to the weak Cenozoic

tectonic activity on the Hainan island, the Taiwan island experienced oblique collision between the Luzon volcanic arc and the Eurasian continent, leading to the rise of the Central Mountain Range of the Taiwan island in the late Miocene (~6.5 Ma) (Sibuet and Hsu, 2004). Therefore, the Hainan and Taiwan islands have different Cenozoic geological backgrounds. Although the central Hainan island has a slow uplift during the Early Pleistocene, rapid uplift occurred on the Taiwan island (Shi et al., 2011; Fox et al., 2014). In addition, the rock strength plays an important role on the erosion rates of the Hainan and Taiwan islands. The Hainan island is occupied by igneous rocks and older strata with higher rock strength (Lin et al., 2017). The Taiwan island is dominated by metamorphic rocks and younger strata with weaker rock strength (Ekka et al., 2023).

In this study, our result compared with the previous studies (Derrieux et al., 2014; Chen et al., 2021) (Table 2) after estimating the lithological erodibility calculation method proposed by Campforts et al. (2020). The result indicates that the lithological erodibility between the Hainan and Taiwan islands has a limited effect on erosion rates. Therefore, despite in the similar climatic backgrounds, the differences in erosion rates between the Hainan and Taiwan islands are primarily influenced by variations in tectonic activities.

6 Conclusions

1. The results of the hypsometric index analysis indicate that the hypsometric curves of the main catchments on the Hainan island has a concave shape with the HI values of less than 0.35, which suggests the Hainan island is at an old-age stage of geomorphic development. The channel steepness index (K_{sn}) analysis of the Hainan island indicates that the main rivers on the island have low K_{sn} values, although higher K_{sn} values are observed in the central region of the island, indicating variations in channel elevation and relatively active tectonic processes in this area. The χ analysis across the catchments shows small variations in χ values on the Hainan island. However, prominent differences in χ values occur at the watershed divides of the Wanquanhe-Nandujiang and Changhuajiang-Nandujiang catchments, which indicates the potential divide migrations occurred in these regions.

2. The results of the cosmogenic nuclide ^{10}Be analysis present the catchment-averaged erosion rates of 35 m/Myr, 42.5 m/Myr and 69.9 m/Myr for the Changhuajiang, Wanquanhe and Lingshuihe catchments, respectively. This indicates that there are low erosion rates on the Hainan island over ten-thousand-year timescales. Therefore, the sediment delivery from the Changhuajiang, Wanquanhe and Lingshuihe catchments of the Hainan island to the Qiongdongnan and Yinggehai Basins in the NW South China Sea is estimated to be 0.46 Mt/yr, 0.45 Mt/yr and 0.21 Mt/yr, respectively. This indicates
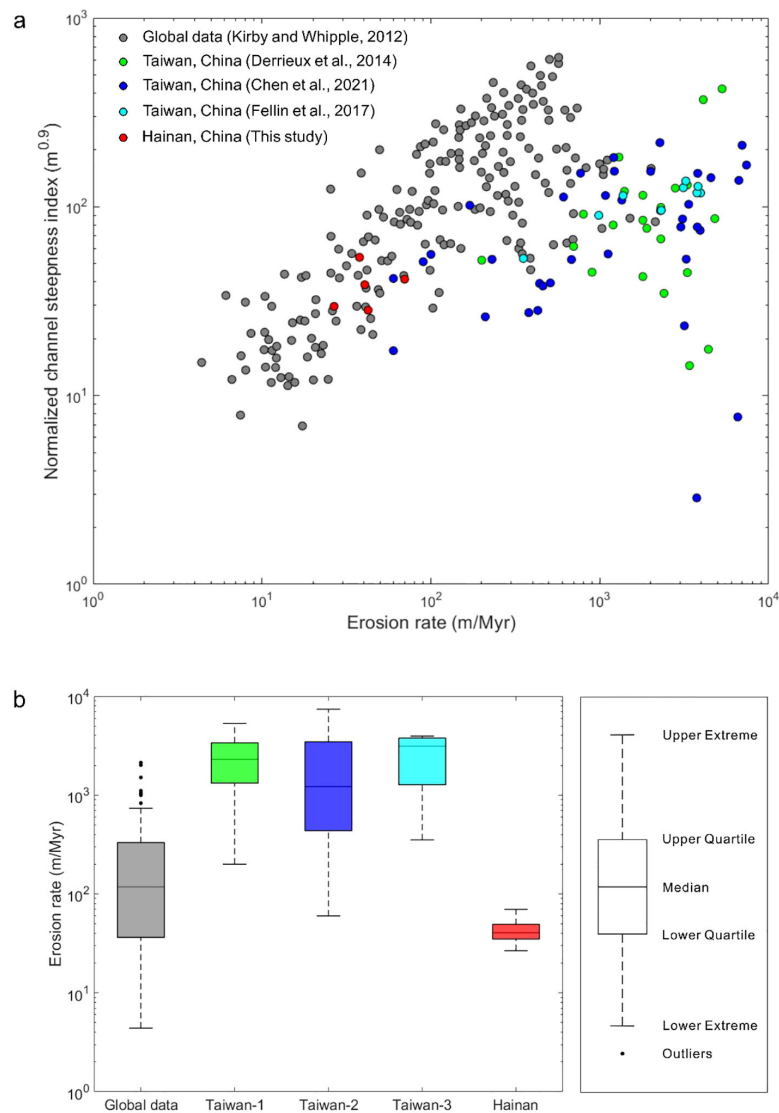
FIGURE 11
(A) Normalized channel steepness index and erosion rates of the Hainan island and global cases. Normalized channel steepness index of the Hainan island and Taiwan island were computed using integral methods, yielding a uniform concavity index of 0.45 consistent with global data; **(B)** Box plots of erosion rates for the Hainan island, Taiwan island and worldwide. Taiwan-1, Taiwan-2, and Taiwan-3 are from Derrieux et al. (2014); Chen et al. (2021) and Fellin et al. (2017), respectively.

TABLE 2 Analysis of Lithological erodibility on the Hainan and Taiwan islands.

Locations	Lithology	Stratum	Lithological erodibility	E(mm/yr)
Hainan	Mudstone、Sandstone	Cretaceous	0.781	0.03
	Granite	Permian	0.286	0.04
	Granite	Triassic	0.286	0.04
	Granite	Cretaceous	0.286	0.07
Taiwan	Shale	Neogene	1.505	1.1
	Pyroclastic	Paleogene	1.448	0.9
	Ultramafic、Gneiss	Precambrian	0.286	22.9
	Pyroclastic	Paleogene	1.448	0.6

small contribution of sedimentary deliveries from the Hainan island during the Quaternary to the Qiongdongnan and Yinggehai Basins.

3. Analysis of the controls of fluvial geomorphology on the Hainan island indicates that the evolution of topography and the distribution of knickpoints are strongly associated with the tectonic uplift, faults, magmatic activity, lithological variations and climate. This study explores that the erosion rates of the Taiwan and Hainan islands in the northern South China Sea are primarily derived from tectonism. The arc-continent collision in the Taiwan island results in higher tectonic uplift.

Data availability statement

The datasets presented in this study can be found in online repositories. The names of the repository/repositories and accession number(s) can be found in the article/Supplementary Material.

Author contributions

KQ: Data curation, Methodology, Software, Writing – original draft. CL: Conceptualization, Data curation, Funding acquisition, Supervision, Writing – review & editing. CT: Data curation, Investigation, Methodology, Software, Writing – original draft. RY: Investigation, Methodology, Writing – review & editing. SW: Conceptualization, Data curation, Writing – review & editing. JR: Conceptualization, Data curation, Funding acquisition, Investigation, Writing – review & editing.

Funding

Acknowledgments

Conflict of interest

The authors declare that the research was conducted in the absence of any commercial or financial relationships that could be construed as a potential conflict of interest.

Publisher's note

All claims expressed in this article are solely those of the authors and do not necessarily represent those of their affiliated organizations, or those of the publisher, the editors and the reviewers. Any product that may be evaluated in this article, or claim that may be made by its manufacturer, is not guaranteed or endorsed by the publisher.

Supplementary material

The Supplementary Material for this article can be found online at: https://www.frontiersin.org/articles/10.3389/fmars.2024.1475481/full#supplementary-material

References

Allen, P. A. (1997). *Earth surface processes* (Oxford: Blackwell Science Ltd).

Allen, P. A., and Allen, J. R. (2013). *Basin analysis : principles and application to petroleum play assessment.* (West Susex, UK: Blackwell Science Ltd).

An, A., Choi, S. H., Yu, Y., and Lee, D. (2017). Petrogenesis of Late Cenozoic basaltic rocks from southern Vietnam. *Lithos* 272-273, 192–204. doi: 10.1016/j.lithos.2016.12.008

Bai, M., Chevalier, M., Pan, J., Replumaz, A., Leloup, P. H., Métois, M., et al. (2018). Southeastward increase of the late Quaternary slip-rate of the Xianshuihe fault, eastern Tibet. Geodynamic and seismic hazard implications. *Earth Planet Sci. Lett.* 485, 19–31. doi: 10.1016/j.epsl.2017.12.045

Bai, S., Cui, Z., and Dang, J. (2009). *Soil mechanics* (Beijing: China Water&Power Press).

Barckhausen, U., Engels, M., Franke, D., Ladage, S., and Pubellier, M. (2014). Evolution of the South China Sea: Revised ages for breakup and seafloor spreading. *Mar. Pet Geol* 58, 599–611. doi: 10.1016/j.marpetgeo.2014.02.022

Baumann, S., Robl, J., Prasicek, G., Salcher, B., and Keil, M. (2018). The effects of lithology and base level on topography in the northern alpine foreland. *Geomorphology (Amst)* 313, 13–26. doi: 10.1016/j.geomorph.2018.04.006

Beeson, H. W., McCoy, S. W., and Keen-Zebert, A. (2017). Geometric disequilibrium of river basins produces long-lived transient landscapes. *Earth Planet Sci. Lett.* 475, 34–43. doi: 10.1016/j.epsl.2017.07.010

Boulton, S. J., and Whittaker, A. C. (2009). Quantifying the slip rates, spatial distribution and evolution of active normal faults from geomorphic analysis: Field examples from an oblique-extensional graben, southern Turkey. *Geomorphology (Amst)* 104, 299–316. doi: 10.1016/j.geomorph.2008.09.007

Campforts, B., Vanacker, V., Herman, F., Vanmaercke, M., Schwanghart, W., Tenorio, G. E., et al. (2020). Parameterization of river incision models requires accounting for environmental heterogeneity: insights from the tropical Andes. *Earth Surf Dyn* 8, 447–470. doi: 10.5194/esurf-8-447-2020

Cao, L., Jiang, T., Wang, Z., Zhang, Y., and Sun, H. (2015). Provenance of Upper Miocene sediments in the Yinggehai and Qiongdongnan basins, northwestern South China Sea: Evidence from REE, heavy minerals and zircon U–Pb ages. *Mar. Geol* 361, 136–146. doi: 10.1016/j.margeo.2015.01.007

Chen, J., Xie, G., and Li, Y. (1991). Modern erosion in hainan island and its comparison with Taiwan island and the hawaiian islands. *Quaternary Sci.* 11, 289–299.

Chen, Y., Sung, Q., and Cheng, K. (2003). Along-strike variations of morphotectonic features in the Western Foothills of Taiwan: tectonic implications based on stream-gradient and hypsometric analysis. *Geomorphology (Amst)* 56, 109–137. doi: 10.1016/S0169-555X(03)00059-X

Chen, C., Willett, S. D., Christl, M., and Shyu, J. B. H. (2021). Drainage basin dynamics during the transition from early to mature orogeny in Southern Taiwan. *Earth Planet Sci. Lett.* 562, 116874. doi: 10.1016/j.epsl.2021.116874

Cheng, C., Kuang, Z., Jiang, T., Cao, L., Ren, J., Liang, J., et al. (2022). Source of the sand-rich gas hydrate reservoir in the northern South China Sea: Insights from detrital zircon U–Pb geochronology and seismic geomorphology. *Mar. Pet Geol* 145, 105904. doi: 10.1016/j.marpetgeo.2022.105904

Christl, M., Vockenhuber, C., Kubik, P. W., Wacker, L., Lachner, J., Alfimov, V., et al. (2013). The ETH Zurich AMS facilities: Performance parameters and reference materials. *Nucl. Instruments Methods Phys. Res. Section B: Beam Interact. Materials Atoms* 294, 29–38. doi: 10.1016/j.nimb.2012.03.004

Clark, M. K., Schoenbohm, L. M., Royden, L. H., Whipple, K. X., Burchfiel, B. C., Zhang, X., et al. (2004). Surface uplift, tectonics, and erosion of eastern Tibet from large-scale drainage patterns. *Tectonics* 23, TC1006. doi: 10.1029/2002TC001402

Clift, P., Lee, G. H., Duc, N. A., Barckhausen, U., Van Long, H., and Zhen, S. (2008). Seismic reflection evidence for a Dangerous Grounds miniplate: No extrusion origin for the South China Sea. *Tectonics* 27, TC3008. doi: 10.1029/2007TC002216

Clift, P. D., and Sun, Z. (2006). The sedimentary and tectonic evolution of the Yinggehai – Song Hong basin and the southern Hainan margin, South China Sea: Implications for Tibetan uplift and monsoon intensification. *J. Geophys Res. Solid Earth* 111, B06405. doi: 10.1029/2005JB004048

Dadson, S. J., Hovius, N., Chen, H., Dade, W. B., Hsieh, M., Willett, S. D., et al. (2003). Links between erosion, runoff variability and seismicity in the Taiwan orogen. *Nature* 426, 648–651. doi: 10.1038/nature02150

Dai, C., Gao, S., Li, G., Zhao, Y., and Tu, J. (2016). Shallow seismic stratigraphic records of Holocene geomorphological dynamics from barrier-lagoons of southeast Hainan Island. *Quaternary Sci.* 36, 57–65. doi: 10.11928/j.issn.1001-7410.2016.05

Davis, W. M. (1899). The geographical cycle. *Geogr. J.* 14, 481–504. doi: 10.2307/1774538

Derrieux, F., Siame, L. L., Bourlès, D. L., Chen, R., Braucher, R., Léanni, L., et al. (2014). How fast is the denudation of the Taiwan mountain belt? Perspectives from *in situ* cosmogenic 10be. *J. Asian Earth Sci.* 88, 230–245. doi: 10.1016/j.jseaes.2014.03.012

Duvall, A., Kirby, E., and Burbank, D. (2004). Tectonic and lithologic controls on bedrock channel profiles and processes in coastal California. *J. Geophys Res. Earth Surf* 109, F03002. doi: 10.1029/2003JF000086

Ekka, S. V., Liang, Y., Huang, K., Huang, J., and Lee, D. (2023). Riverine molybdenum isotopic fractionation in small mountainous rivers of Taiwan: the effect of chemical weathering and lithology. *Chem. Geol* 620, 121349. doi: 10.1016/j.chemgeo.2023.121349

Fellin, M. G., Chen, C., Willett, S. D., Christl, M., and Chen, Y. (2017). Erosion rates across space and timescales from a multi-proxy study of rivers of eastern Taiwan. *Glob Planet Change* 157, 174–193. doi: 10.1016/j.gloplacha.2017.07.012

Flint, J. J. (1974). Stream gradient as a function of order, magnitude, and discharge. *Water Resour Res.* 10, 969–973. doi: 10.1029/WR010i005p00969

Fox, M., Goren, L., May, D. A., and Willett, S. D. (2014). Inversion of fluvial channels for paleorock uplift rates in Taiwan. *J. Geophysical Research: Earth Surface* 119, 1853–1875. doi: 10.1002/2014JF003196

Gallen, S. F., and Wegmann, K. W. (2017). River profile response to normal fault growth and linkage: an example from the Hellenic forearc of south-central Crete, Greece. *Earth Surf Dyn* 5, 161–186. doi: 10.5194/esurf-5-161-2017

Goren, L., Willett, S. D., Herman, F., and Braun, J. (2014). Coupled numerical analytical approach to landscape evolution modeling. *Earth Surf Process Landf* 39, 522–545. doi: 10.1002/esp.3514

Granger, D. E., Kirchner, J. W., and Finkel, R. C. (1997). Quaternary downcutting rate of the New River, Virginia, measured from differential decay of cosmogenic 26Al and 10be in cave-deposited alluvium. *Geology* 25, 107–110. doi: 10.1130/0091-7613(1997)025<0107:QDROTN>2.3.CO;2

Hack, J. T. (1957). Studies of longitudinal stream profiles in Virginia and Maryland. doi: 10.3133/pp294B

Harel, M. A., Mudd, S. M., and Attal, M. (2016). Global analysis of the stream power law parameters based on worldwide 10be denudation rates. *Geomorphology (Amst)* 268, 184–196. doi: 10.1016/j.geomorph.2016.05.035

Horton, B. K. (2018). Sedimentary record of Andean mountain building. *Earth Sci. Rev.* 178, 279–309. doi: 10.1016/j.earscirev.2017.11.025

Howard, A. D. (1965). Geomorphological systems—Equilibrium and dynamics. *Am. J. Sci.* 263, 302–312. doi: 10.2475/ajs.263.4.302

Hu, Y., Hao, M., Ji, L., and Song, S. (2016). Three-dimensional crustal movement and the activities of earthquakes, volcanoes and faults in Hainan Island, China. *Geod Geodyn* 7, 284–294. doi: 10.1016/j.geog.2016.05.008

Hu, Y., Hao, M., Qin, S., Ji, L., and Song, S. (2018). Present-day 3D crustal motion and fault activity in the Hainan island. *Chin. J. Geophys-Chinese Ed* 61, 2310–2321. doi: 10.6038/cjg2018L0274

Institute, H. G. S. (2017). *The regional geology of China : hainan* (Beijing: Geology Press).

Jepson, G., Carrapa, B., Gillespie, J., Feng, R., DeCelles, P. G., Kapp, P., et al. (2021). Climate as the great equalizer of continental-scale erosion. *Geophys Res. Lett.* 48, e2021GL095008. doi: 10.1029/2021GL095008

Jiang, X., Dilek, Y., and Li, X. (2024). Cretaceous magmatic arc in Hainan and the peri-South China Sea as evidenced by geochemical fingerprinting of granitoids in the region. *Geosci Front.* 15, 101866. doi: 10.1016/j.gsf.2024.101866

Jiang, X., Ren, F., Li, Y., Qiu, W., Cai, Z., and Ma, Q. (2018). Characteristics and preliminary causes of tropical cyclone extreme rainfall events over hainan island. *Adv. Atmospheric Sci.* 35, 580–591. doi: 10.1007/s00376-017-7051-0

Kirby, E., and Whipple, K. X. (2012). Expression of active tectonics in erosional landscapes. *J. Struct. Geol* 44, 54–75. doi: 10.1016/j.jsg.2012.07.009

Kirby, E., Whipple, K. X., Tang, W., and Chen, Z. (2003). Distribution of active rock uplift along the eastern margin of the Tibetan Plateau: Inferences from bedrock channel longitudinal profiles. *J. Geophys Res. Solid Earth* 108, 2217. doi: 10.1029/2001JB000861

Kubik, P. W., and Christl, M. (2010). 10be and 26Al measurements at the Zurich 6 MV Tandem AMS facility. *Nucl. Instruments Methods Phys. Res. Section B: Beam Interact. Materials Atoms* 268, 880–883. doi: 10.1016/j.nimb.2009.10.054

Lague, D. (2014). The stream power river incision model: evidence theory and beyond. *Earth Surf Process Landf* 39, 38–61. doi: 10.1002/esp.3462

Lal, D. (1991). Cosmic ray labeling of erosion surfaces: *in situ* nuclide production rates and erosion models. *Earth Planet Sci. Lett.* 104, 424–439. doi: 10.1016/0012-821X(91)90220-C

Lei, C. (2012). *Structure and evolution of yinggehai and qiongdongnan basins, south China sea: implications for cenozoic tectonics in southeast asia.* (Wuhan: China University of Geosciences).

Lei, C., Alves, T. M., Ren, J., and Tong, C. (2020). Rift Structure and Sediment Infill of Hyperextended Continental Crust: Insights From 3D Seismic and Well Data (Xisha Trough, South China Sea). *J. Geophysical Research: Solid Earth* 125, e2019JB018610. doi: 10.1029/2019JB018610

Lei, C., Ren, J., Pei, J., Liu, B., Zuo, X., and Zhu, J. L. S. (2021). Tectonics of the offshore Red River Fault recorded in the junction of the Yinggehai and Qiongdongnan Basins. *Sci. China Earth Sci.* 64, 1893–1908. doi: 10.1007/s11430-020-9796-2

Lei, C., Ren, J., Sternai, P., Fox, M., Willett, S., Xie, X., et al. (2015). Structure and sediment budget of Yinggehai–Song Hong basin, South China Sea: Implications for Cenozoic tectonics and river basin reorganization in Southeast Asia. *Tectonophysics* 655, 177–190. doi: 10.1016/j.tecto.2015.05.024

Lei, J., Zhao, D., Steinberger, B., Wu, B., Shen, F., and Li, Z. (2009). New seismic constraints on the upper mantle structure of the Hainan plume. *Phys. Earth Planet Inter* 173, 33–50. doi: 10.1016/j.pepi.2008.10.013

Li, G., Zhou, L., Qi, Y., and Gao, S. (2019). Threshold sediment flux for the formation of river deltas in Hainan Island, southern China. *J. Geogr. Sci.* 29, 146–160. doi: 10.1007/s11442-019-1589-y

Li, Z., Wang, X., Yu, Y., Zhang, H., Su, Q., Miao, X., et al. (2021). The impacts of base level and lithology on fluvial geomorphic evolution at the tectonically active Laohu and Hasi Mountains, northeastern Tibetan Plateau. *Sci. China Earth Sci.* 64, 906–919. doi: 10.1007/s11430-020-9743-1

Liang, D., Wu, S., Xu, G., Xia, C., Gao, F., Lin, Y., et al. (2023a). Paleoenvironmental changes in the coastal zone of the northwest South China Sea during the last 13 kyr. *Sci. Rep.* 13, 13540. doi: 10.1038/s41598-023-40721-5

Liang, D., Xu, G., Gao, F., Wen, L., Jia, L., Liu, L., et al. (2023b). Holocene sediment source analysis and paleoclimatic significance of core KZK01 from the eastern part of the Beibu Gulf. *Front. Mar. Sci.* 11. doi: 10.3389/feart.2023.1192206

Lifton, N. A., and Chase, C. G. (1992). Tectonic, climatic and lithologic influences on landscape fractal dimension and hypsometry: implications for landscape evolution in the San Gabriel Mountains, California. *Geomorphology (Amst)* 5, 77–114. doi: 10.1016/0169-555X(92)90059-W

Lin, M. (1995). Submarine geomorphology of the eastern continental shelf of the hainan island. *Mar. Geology Quaternary Geology* 15, 37–46. doi: 10.16562/j.cnki.0256-1492.1995.04.004

Lin, Y., Lyu, Z., Yuan, Q., Wang, C., Guan, J., and Hu, Z. (2017). Geochemistry and tectonic setting of the Early Cretaceous volcanics in Wuzhishan area, Hainan Island, South China. *Geology Mineral Resour. South China* 33, 215–228. doi: 10.3969/j.issn.1007-3701.2017.03.003

Lin, A. T., Watts, A. B., and Hesselbo, S. P. (2003). Cenozoic stratigraphyand subsidencehistoryof the South China Seamargin in theTaiwan region. *Basin Res.* 15, 453–478. doi: 10.1046/j.1365-2117.2003.00215.x

Liu, E., Yan, D., Pei, J., Lin, X., and Zhang, J. (2023). Sedimentary architecture and evolution of a Quaternary sand-rich submarine fan in the South China Sea. *Front. Mar. Sci.* 10. doi: 10.3389/fmars.2023.1280763

Liu, Z., Zhao, Y., Colin, C., Stattegger, K., Wiesner, M. G., Huh, C., et al. (2016). Source-to-sink transport processes of fluvial sediments in the South China Sea. *Earth Sci. Rev.* 153, 238–273. doi: 10.1016/j.earscirev.2015.08.005

Loget, N., and Van Den Driessche, J. (2009). Wave train model for knickpoint migration. *Geomorphology (Amst)* 106, 376–382. doi: 10.1016/j.geomorph.2008.10.017

Milliman, J. D., and Farnsworth, K. L. (2011). *River discharge to the coastal ocean: a global synthesis.* (Cambridge: Cambridge University Press).

Montelli, R., Nolet, G., Dahlen, F. A., and Masters, G. (2006). A catalogue of deep mantle plumes: New results from finite-frequency tomography. *Geochem Geophys Geosyst* 7, 11. doi: 10.1029/2006GC001248

Pang, L., Lu, H., Lü, Y., Jiang, Y., Wu, D., Wu, M., et al. (2022). 10be dating of the Kuitun River terraces in the northern Chinese Tian Shan foreland: Insights into fluvial evolution and tectonic shortening pattern. *Geomorphology (Amst)* 412, 108317. doi: 10.1016/j.geomorph.2022.108317

Penserini, B. D., Morell, K. D., Codilean, A. T., Fülöp, R., Wilcken, K. M., Yanites, B. J., et al. (2024). Magnitude and timing of transient incision resulting from large-scale drainage capture, Sutlej River, Northwest Himalaya. *Earth Surf Process Landf* 49, 334–353. doi: 10.1002/esp.5705

Perron, J. T., and Royden, L. (2013). An integral approach to bedrock river profile analysis. *Earth Surf Process Landf* 38, 570–576. doi: 10.1002/esp.3302

Pike, R. J., and Wilson, S. E. (1971). Elevation-relief ratio, hypsometric integral, and geomorphic area-altitude analysis. *Geol Soc. Am. Bull.* 82, 1079–1084. doi: 10.1130/0016-7606(1971)82[1079:ERHIAG]2.0.CO;2

Romans, B. W., Castelltort, S., Covault, J. A., Fildani, A., and Walsh, J. P. (2016). Environmental signal propagation in sedimentary systems across timescales. *Earth Sci. Rev.* 153, 7–29. doi: 10.1016/j.earscirev.2015.07.012

Schwanghart, W., and Scherler, D. (2014). TopoToolbox 2 – MATLAB-based software for topographic analysis and modeling in Earth surface sciences. *Earth Surf Dyn* 2, 1–7. doi: 10.5194/esurf-2-1-2014

Schwanghart, W., and Scherler, D. (2017). Bumps in river profiles: uncertainty assessment and smoothing using quantile regression techniques. *Earth Surf Dyn* 5, 821–839. doi: 10.5194/esurf-5-821-2017

Shi, X., Kohn, B., Spencer, S., Guo, X., Li, Y., Yang, X., et al. (2011). Cenozoic denudation history of southern Hainan Island, South China Sea: Constraints from low temperature thermochronology. *Tectonophysics* 504, 100–115. doi: 10.1016/j.tecto.2011.03.007

Sibuet, J., and Hsu, S. (2004). How was Taiwan created? *Tectonophysics* 379, 159–181. doi: 10.1016/j.tecto.2003.10.022

Sklar, L. S., and Dietrich, W. E. (2001). Sediment and rock strength controls on river incision into bedrock. *Geology* 29, 1087–1090. doi: 10.1130/0091-7613(2001)029<1087:SARSCO>2.0.CO;2

Sømme, T. O., Helland-Hansen, W., Martinsenw, O. J., and Thurmond, J. B. (2009a). Relationships between morphological and sedimentological parameters in source-to-sink systems: a basis for predicting semi-quantitative characteristics in subsurface systems. *Basin Res.* 21, 361–387. doi: 10.1016/j.geomorph.2020.107441

Sømme, T. O., Martinsen, O. J., and Thurmond, J. B. (2009b). Reconstructing morphological and depositional characteristics in subsurface sedimentary systems: an example from the Maastrichtian–Danian Ormen Lange system, Møre Basin, Norwegian Sea. *Am. Assoc. Pet Geol Bull.* 93, 1347–1377. doi: 10.1306/06010909038

Sonam, S., Singh, R. N., and Jain, V. (2021). Temporal profiling of uplift rate along an active fault using river long profile in the Kuchchh region, Western India. *Quat Int.* 585, 85–98. doi: 10.1016/j.quaint.2020.11.022

Strahler, A. N. (1952). Hypsometric (area-altitude) analysis of erosional topography. *Geol Soc. Am. Bull.* 63, 1117–1141. doi: 10.1130/0016-7606(1952)63[1117:HAAOET]2.0.CO;2

Syvitski, J. P. M., and Milliman, J. D. (2007). Geology, geography, and humans battle for dominance over the delivery of fluvial sediment to the coastal ocean. *J. Geol* 115, 1–19. doi: 10.1086/509246

Vergara, I., Garreaud, R., Araneo, D., and Leyton, F. (2023). Environmental control of the present-day sediment export along the extratropical Andes. *Geomorphology (Amst)* 441, 108911. doi: 10.1016/j.geomorph.2023.108911

von Blanckenburg, F. (2005). The control mechanisms of erosion and weathering at basin scale from cosmogenic nuclides in river sediment. *Earth Planet Sci. Lett.* 237, 462–479. doi: 10.1016/j.epsl.2005.06.030

Walsh, L. S., Martin, A. J., Ojha, T. P., and Fedenczuk, T. (2012). Correlations of fluvial knickzones with landslide dams, lithologic contacts, and faults in the southwestern Annapurna Range, central Nepalese Himalaya. *J. Geophys Res. Earth Surf* 117, F01012. doi: 10.1029/2011JF001984

Wang, X., Li, Z., Li, X., Li, J., Xu, Y., and Li, X. (2013). Identification of an ancient mantle reservoir and young recycled materials in the source region of a young mantle plume: Implications for potential linkages between plume and plate tectonics. *Earth Planet Sci. Lett.* 377-378, 248–259. doi: 10.1016/j.epsl.2013.07.003

Wang, C., Liang, X., Foster, D. A., Xie, Y., Tong, C., Pei, J., et al. (2016). Zircon U-Pb geochronology and heavy mineral composition constraints on the provenance of the middle Miocene deep-water reservoir sedimentary rocks in the Yinggehai-Song Hong Basin, South China Sea. *Mar. Pet Geol* 77, 819–834. doi: 10.1016/j.marpetgeo.2016.05.009

Wang, C., Liang, X., Xie, Y., Tong, C., Pei, J., Zhou, Y., et al. (2014). Provenance of Upper Miocene to Quaternary sediments in the Yinggehai-Song Hong Basin, South

China Sea: Evidence from detrital zircon U–Pb ages. *Mar. Geol* 355, 202–217. doi: 10.1016/j.margeo.2014.06.004

Wang, W., and Ou, X. (1986). The dynamics and topographic development of the nandujiang estuary. *Tropic Oceanology* 5, 80–88. doi: CNKI:SUN:RDHY.0.1986-04-010

Wang, C., Zeng, L., Lei, Y., He, J., Cui, H., and Su, M. (2021). Geochemical record of the sediments in the continental shelf of the northwestern South China Sea: Implications for the provenance and sedimentary evolution. *Mar. Geol* 440, 106582. doi: 10.1016/j.margeo.2021.106582

Whipple, K. X. (2001). Fluvial landscape response time: How plausible is steady-state denudation? *Am. J. Sci.* 301, 313–325. doi: 10.2475/ajs.301.4-5.313

Whipple, K. X. (2004). Bedrock rivers and the geomorphology of active orogens. *Annu. Rev. Earth Planet Sci.* 32, 151–185. doi: 10.1146/annurev.earth.32.101802.120356

Whipple, K. X., Forte, A. M., DiBiase, R. A., Gasparini, N. M., and Ouimet, W. B. (2017). Timescales of landscape response to divide migration and drainage capture: Implications for the role of divide mobility in landscape evolution. *J. Geophysical Research: Earth Surface* 122, 248–273. doi: 10.1002/2016JF003973

Whipple, K. X., Hancock, G. S., and Anderson, R. S. (2000). River incision into bedrock: Mechanics and relative efficacy of plucking, abrasion, and cavitation. *Geol Soc. Am. Bull.* 112, 490–503. doi: 10.1130/0016-7606(2000)112<490:RIIBMA>2.0.CO;2

Whipple, K. X., and Tucker, G. E. (1999). Dynamics of the stream-power river incision model: Implications for height limits of mountain ranges, landscape response timescales, and research needs. *J. Geophysical Research: Solid Earth* 104, 17661–17674. doi: 10.1029/1999JB900120

Whittaker, A. C. (2012). How do landscapes record tectonics and climate? *Lithosphere* 4, 160–164. doi: 10.1130/RF.L003.1

Willett, S. D., McCoy, S. W., Perron, J. T., Goren, L., and Chen, C. (2014). Dynamic reorganization of river basins. *Science* 343, 1248765. doi: 10.1126/science.1248765

Wobus, C., Whipple, K. X., Kirby, E., Snyder, N., Johnson, J., Spyropolou, K., et al. (2006). Tectonics from topography: Procedures, promise, and pitfalls. *Tectonics Climate Landscape Evol.* 398, 55–74. doi: 10.1130/2006.2398(04)

Wu, L., Prush, V., Lin, X., Xiao, A., Zhang, L., Chen, N., et al. (2019). Quantifying wind erosion during the late quaternary in the qaidam basin, central asia. *Geophys Res. Lett.* 46, 6378–6387. doi: 10.1029/2019GL082992

Xia, S., Fan, C., Sun, J., Cao, J., Zhao, F., and Wan, K. (2017). Characteristics of Late Cenozoic Magmatic Activities on the Northern Margin of South Chian Sea and their Tectonic Implications. *Mar. Geology Quaternary Geology* 37, 25–33. doi: 10.16562/j.cnki.0256-1492.2017.06.003

Xu, F., Zhang, Y., Hu, B., Cui, R., Zhang, L., Huang, W., et al. (2024). Evolution of the sedimentary environment on the continental shelf of southeastern Hainan Island under the influences of sea level and climate during the Holocene. *J. Asian Earth Sci.* 263, 106023. doi: 10.1016/j.jseaes.2024.106023

Yan, Q., and Shi, X. (2007). Hainan mantle plume and the formation and evolution of the south China sea. *Geological J. China Universities* 13, 311–322. doi: 10.16108/j.issn1006-7493.2007.02.014

Yan, Q., Shi, X., Yang, Y., and Wang, K. (2008). Potassium-argon/argon-40-argon-39 geochronology of Cenozoic alkali basalts from the South China Sea. *Hai Yang Xue Bao* 27, 115–123. doi: CNKI:SUN:SEAE.0.2008-06-013

Yang, R., and Goren, S. D. W. L. (2015). *In situ* low-relief landscape formation as a result of river network disruption. *Nature* 520, 526–529. doi: 10.1038/nature14354

Zhang, Z., Daly, J. S., Tian, Y., Tyrrell, S., Sun, X., Badenszki, E., et al. (2022a). Sedimentary provenance perspectives on the evolution of the major rivers draining the eastern Tibetan Plateau. *Earth Sci. Rev.* 232, 104151. doi: 10.1016/j.earscirev.2022.104151

Zhang, Z., Daly, J. S., Yan, Y., Badenszki, E., Sun, X., and Tian, Y. (2022b). Cenozoic reorganization of fluvial systems in eastern China: Sedimentary provenance of detrital K-feldspar in Taiwan. *Chem. Geol* 592, 120740. doi: 10.1016/j.chemgeo.2022.120740

Zhang, J., Tian, Q., Li, F., Gao, Z., and Su, G. (2008). Study on neotectonic characteristics and its evolution in northwestern Hainan Island. *Earthquake* 28, 85–94. doi: 10.3969/j.issn.1000-3274.2008.03.012

Zhang, Y., Yu, K., Fan, T., Yue, Y., Wang, R., Jiang, W., et al. (2020). Geochemistry and petrogenesis of Quaternary basalts from Weizhou Island, northwestern South China Sea: Evidence for the Hainan plume. *Lithos* 362-363, 105493. doi: 10.1016/j.lithos.2020.105493

Zhang, Y., Zhang, H., Ma, Z., Wang, Y., and Zhao, X. (2023). Inversion of Late Miocene uplift history from the transient Daxia River landscape, NE Tibetan Plateau. *J. Geol Soc. London* 180, jgs2023–jgs2030. doi: 10.1144/jgs2023-030

Zhao, D. (2007). Seismic images under 60 hotspots: Search for mantle plumes. *Gondwana Res.* 12, 335–355. doi: 10.1016/j.gr.2007.03.001

Zhao, D., Toyokuni, G., and Kurata, K. (2021). Deep mantle structure and origin of Cenozoic intraplate volcanoes in IndoChina, Hainan and South China Sea. *Geophys J. Int.* 225, 572–588. doi: 10.1093/gji/ggaa605

Zhou, D., Ru, K., and Chen, H. (1995). Kinematics of Cenozoic extension on the South China Sea continental margin and its implications for the tectonic evolution of the region. *Tectonophysics* 251, 161–177. doi: 10.1016/0040-1951(95)00018-6

Zhou, L., Yang, Y., Li, G., and Tong, C. (2023). OSL dating of coastal dunes on the southeastern coast of Hainan Island, China. *Front. Mar. Sci.* 10, 1165551. doi: 10.3389/fmars.2023.1165551